Journal of Engineering and Technological Sciences

Research Paper

Combustion Characteristics of High Concentration Ammonia/Ethanol Blends under Varied Boost Pressures in a Spark-assisted Compression Ignition Engine with a Sub-chamber

Takanobu Okada[1], Mitsuhisa Ichiyanagi[2], Emir Yilmaz[2], Rizal Mahmud[2], Christian Dennis Marcelo[1], Ferdinand Ronaldo Tjiotijono[1], Evan Widjaja[3], Jason Sutedjo[3], Gabriel Jeremy Gotama[4], Willyanto Anggono[3,4,*], & Takashi Suzuki[2]

[1]Graduate School of Science and Technology, Sophia University, 7-1 Kioi-cho, Chiyoda-ku, Tokyo 102-8554, Japan
[2]Department of Engineering and Applied Sciences, Faculty of Science and Technology, Sophia University, 7-1 Kioi-cho, Chiyoda-ku, Tokyo 102-8554, Japan
[3]Mechanical Engineering Department, Faculty of Industrial Technology, Petra Christian University, Jalan Siwalankerto 121-131, Surabaya 60236, Indonesia
[4]Centre for Sustainable Energy Studies, Petra Christian University, Jalan Siwalankerto 121-131, Surabaya 60236, Indonesia

*Corresponding author: willy@petra.ac.id

Abstract

Ammonia (NH_3) is a promising carbon-free fuel that offers higher volumetric energy density and easier transport than hydrogen. However, its direct combustion is limited by its slow burning rates and high ignition temperatures. Co-firing with a more reactive fuel, such as ethanol, can overcome these limitations. In this study, the combustion of ammonia/ethanol blends was evaluated in a customized spark-assisted compression ignition (SACI) engine featuring a sub-chamber and a 17.7 compression ratio. The experimental investigation focused on the interaction between boost pressures (5 to 15 kPa) and ammonia energy ratios (50% and 60%) at 1000 rpm and an excess air ratio of 1.2. The results suggest that increasing boost pressure reduced the thermal efficiency and indicated mean effective pressure (IMEP). Accordingly, this resulted in a lower in-cylinder pressure and heat release rate, which slowed down the combustion process. Such unusual behaviour can be attributed to an increase in the latent heat of vaporization of ethanol with pressure, which requires more heat energy for fuel vaporization and effectively cools the combustion chamber. Furthermore, while adopting lower ammonia energy ratios improved engine performance, it resulted in higher NO_x emissions due to the lack of unburned NH_3 in the exhaust to undergo the thermal $DeNO_x$ process, suggesting the need for careful adjustment of the boost pressure and ammonia energy ratio for the practical application of ammonia/ethanol fuels in combustion engines.

Keywords: *ammonia; co-combustion; engine performance; ethanol; boost pressure; sub-chamber.*

Introduction

Climate change has become one of the most pressing environmental challenges worldwide. The primary driver of this phenomenon is the accumulation of greenhouse gases in the atmosphere, with carbon dioxide (CO_2) accounting for approximately 65% of these emissions, making it the most significant contributor to climate change (United States Environmental Protection Agency, 2023). Currently, the transportation sector remains heavily reliant on fossil fuels such as gasoline and diesel, which are the major sources of CO_2 emissions. Although electric vehicles (EVs) are a promising solution for reducing carbon footprints, their widespread adoption is hindered by several limitations, including inadequate charging infrastructure and the relatively low energy density of batteries. Given these constraints, there is a growing interest in exploring alternative fuels that can deliver energy without contributing to CO_2 emissions (Hu et al., 2024; Sonawane et al., 2025).

Previous studies have explored alternative fuels such as hydrogen (Sapnken et al., 2024), biofuels (Kumar et al., 2024), and ammonia (Mohammed et al., 2024). Since hydrogen combustion mainly produces water (H_2O), it is considered the most appealing of the three methods. However, the biggest challenges with hydrogen are its storage (Hamedani &

Copyright by authors ©2026 Published by IRCS - ITB
ISSN: 2337-5779
J. Eng. Technol. Sci. Vol. 58, No. 6, 2026, 745-761
DOI: 10.5614/j.eng.technol.sci.2026.58.6.1

Abbasian, 2024) and transportation (Moriarty & Honnery, 2019) as extreme pressure and temperature are required to handle hydrogen economically. In contrast, ammonia can be easily transported, has a higher volumetric energy density than hydrogen (Brandon & Smith, 2021), and has a well-established supply chain owing to its widespread use in the agricultural sector. Therefore, the practical use of hydrogen is often associated with its conversion into ammonia, which acts as a hydrogen carrier (Sun et al., 2024).

Nonetheless, despite its potential as a substitute for fossil fuels, ammonia has several drawbacks when used directly as an engine fuel such as high ignition resistance (Lanni & Rossi, 2022) and slow laminar burning speed (Hayakawa et al., 2015). Given these challenges, researchers have devised methods to improve the performance of ammonia-fueled engines, such as using an engine sub-chamber (Guo et al., 2022; Ichiyanagi et al., 2024a; Ichiyanagi et al., 2024b; Yilmaz et al., 2023) and blending it with more reactive fuels. In addition to the aforementioned approaches, multiple spark plugs have been implemented to combat the combustibility issue of ammonia (Lanni et al., 2025; Uddeen et al., 2023). The results from these experiments prove that increasing the number of spark plugs helps create more initial flame kernels and improves the subsequent combustion process. In addition, the use of plasma-assisted ignition for the combustion of pure ammonia has been introduced to improve the overall combustibility (Zhang et al., 2025). This approach differs from the usual dual-fuel combustion solution, where the results show that plasma-assisted ignition can achieve relatively stable combustion of pure ammonia, as proven by the coefficient of variation (CoV) of the indicated mean effective pressure (IMEP). However, the application of these ignition strategies is limited. Even though the use of multiple spark plugs improves flame propagation at the start of combustion, it does not fundamentally overcome the low reactivity of ammonia. The application of plasma-assisted ignition is hindered by the complexity of implementing this technology and the large energy consumption required to generate plasma, resulting in lower energy efficiency overall. Considering the drawbacks of these less conventional methods, the use of a dual-fuel strategy remains a more practical approach, and studies have shown improved combustion through blending with gasoline (Ding et al., 2025), kerosene (Zhu et al., 2024), and alcohols such as ethanol (Li et al., 2024; Uddeen et al., 2024). Among these, pairing with ethanol reduces carbon dioxide emissions because ethanol contains fewer carbon atoms and can be produced in a renewable and sustainable manner (Shih et al., 2018). Furthermore, studies have demonstrated the advantages of blending ammonia with ethanol, such as lower knock propensity and reduced pressure oscillations due to the high octane number of ammonia, which suggests a synergy between the two fuels, where ethanol enhances ammonia combustion, while ammonia helps to maintain stable ethanol combustion (Meng et al., 2024). The research on ammonia/ethanol fuel blends can be further complemented by this study, which focuses on the use of higher ammonia energy ratios and the addition of boost pressure for the intake conditions.

The synergy between the two fuels has motivated previous studies to investigate ammonia/ethanol combustion under boosted conditions (Pelé et al., 2024) or when operated in a spark-assisted compression ignition (SACI) engine with a sub-chamber (Okada et al., 2025). However, only a few studies have explored their simultaneous effects on ammonia/ethanol combustion. In addition, the use of ethanol as a combustion promoter presents a number of drawbacks, such as severe charge cooling, reduced energy density, and mixture dilution, because of the presence of oxygen. These effects, particularly at high ammonia ratios, can reduce engine performance and impede the overall combustion process. Techniques such as intake heating, boosting, improved injection, and sophisticated ignition systems are required to overcome these obstacles and maximize the positive effects of ethanol while minimizing its negative effects. In line with the proposed solutions, in this study, we investigated the effect of boost pressure on the combustion of ammonia/ethanol blends with high ammonia energy ratios. This study focused on investigating blends with ammonia energy ratios of 50 and 60% with boost pressures of 5, 10, and 15 kPa. By examining these parameters, this study sought to optimize the use of ammonia/ethanol blends in practical engine applications, contributing to the development of cleaner and more efficient energy solutions.

Experimental Methods

Experimental Setup

We employed a modified diesel engine (YANMAR TF120V) with the configurations shown in Figure 1, and its specifications are provided in Table 1 (Yilmaz et al., 2023). The overall system included a fuel delivery system, oxygen/NO_x sensors, water-cooling mechanism, catalyst, intake/exhaust system, data acquisition setup, system for controlling temperature and pressure, and sub-chamber. The displacement of the engine was 6.38×10^{-4} m^3. The piston had a stroke of 9.6×10^{-2} m along with a diameter of 9.2×10^{-2} m. The sub-chamber had an opening size of 5.26×10^{-5} m^2 and was integrated into the main combustion chamber, which had a volume of 23.5×10^{-6} m^3. The geometry of the sub-chamber is defined as a sphero-cylinder, comprising a central cylinder (height = 8.0×10^{-3} m, radius = 1.6×10^{-2} m)

DOI: 10.5614/j.eng.technol.sci.2026.58.6.1

capped at both ends by hemispheres of the same radius. With a compression ratio of 17.7, this engine delivered nearly double the power of a conventional spark ignition (SI) engine. An ammonia injector (Nikki O-RING Type) and an ethanol injector (BOSCH INJ-035) connected to the ethanol and ammonia fuel tanks were replaced from the sub-chamber and positioned at the intake manifold. Ammonia was injected in gaseous form at a supply pressure of 400 kPa. Ethanol was injected at a pressure of 300 kPa and temperature of 298 K. The top of the sub-chamber was fitted with a spark plug (NGK-SRM) and the mixture supply to the sub-chamber originated only from the main chamber. The pressure variations in the main combustion chamber were tracked using a pressure sensor (Kistler 6054BR-3-1). The engine was connected to an electromagnetic clutch that controlled the engine speed using an eddy current dynamometer. The throttle valve was adjusted manually to maintain a steady intake pressure. A sensor was used to record the intake pressure. The engine control unit (ECU, INFINITY SERIES 7) processed the signals sent to the data logger and regulated the amount of fuel and the ratio as well as the time of fuel injection and ignition. A rotary encoder tracked the location of the piston during combustion by transmitting a top dead center (TDC) signal every two crankshaft rotations to the ECU. Raw pressure data were used to acquire the in-cylinder pressure data in synchronization with the rotary encoder. The exhaust system was equipped with nitrogen oxide (NO_x) and oxygen sensors (Horiba MEXA-720NO_x) to monitor the engine emissions. This sensor was placed upstream of the catalyst to measure only the effects of combustion without the influence of the catalyst. Table 2 lists the models and measurement errors of the instruments used in the experiments. The cooling system included a heat exchanger, pump, coolant heater, and temperature sensors that tracked the coolant temperatures. The exhaust line was equipped with a catalyst to eliminate unburned gas from the combustion. In this study, the boost pressure is defined as the increase in the intake manifold pressure relative to the naturally aspirated condition, with boost levels set at 5, 10, and 15 kPa above the baseline (naturally aspirated condition). In general, the manifold pressure is expressed as the absolute pressure, whereas the boost pressure is based on the gauge pressure. The boost pressure was measured at the intake manifold using a calibrated pressure sensor. All operating parameters, including the engine speed, excess air ratio, and ignition timing, were maintained constant across all test conditions. Additional details regarding the fuel injection system, sub-chamber configuration, and data acquisition procedures are included in this paper to ensure reproducibility of the data.

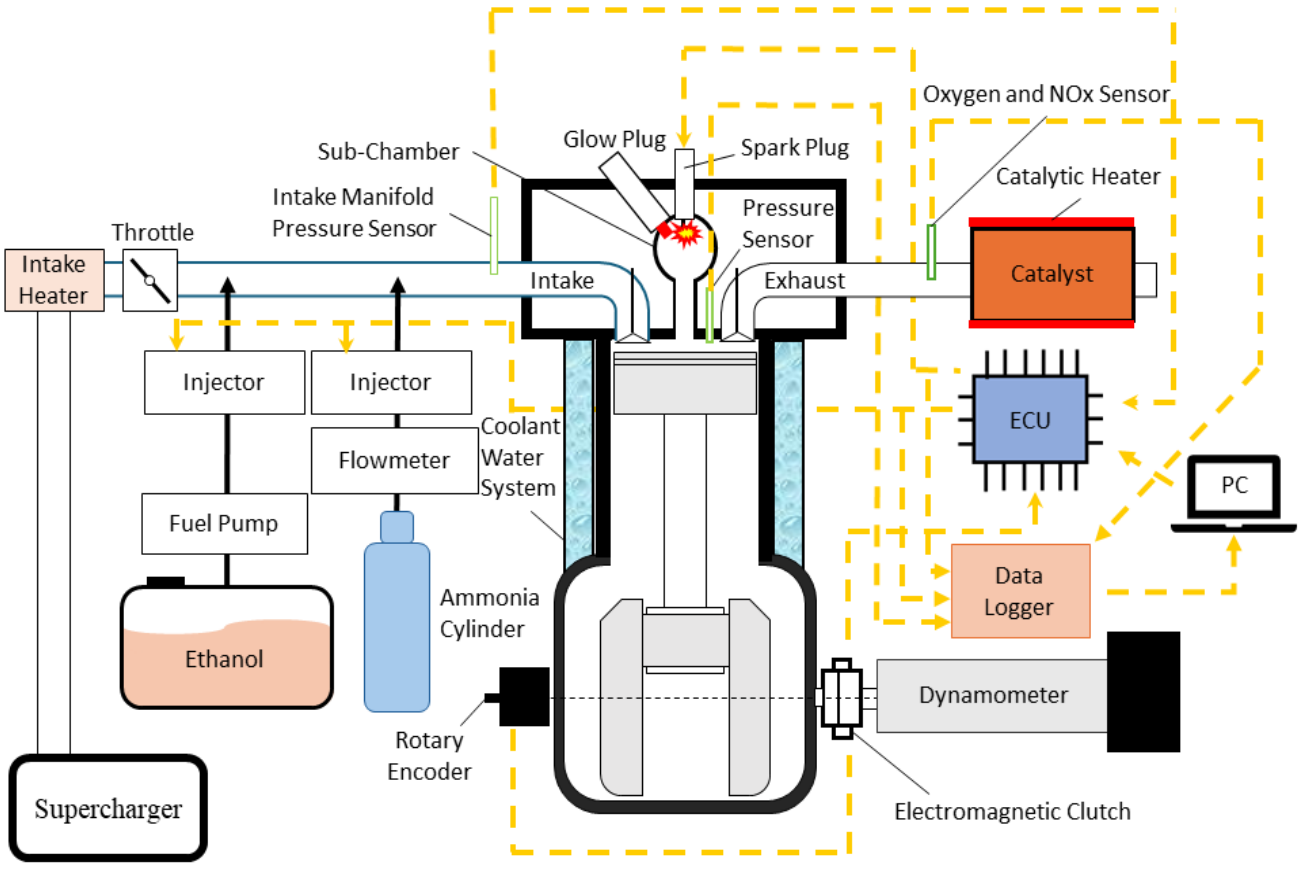


Figure 1 Schematic of the engine experimental setup.

Table 1 Specifications of the engine used in the experiments.

Type of Engine Used [-]	Single-cylinder Horizontal-oriented Diesel Engine
Max. Speed [rpm]	2400
Engine Model [-]	YANMAR TF 120V - E
Ignition Method [-]	Spark Ignition
Valve Mechanism [-]	Overhead Valve
Type of Aspiration [-]	Boosted Intake
Fuel Injection Method [-]	Port Injection
Total Displacement [m³]	6.38×10^{-4}
Compression Ratio [-]	17.7
Bore × Stroke [m]	9.2×10^{-2} x 9.6×10^{-2}
Sub-chamber [-]	Spherical Swirl
Sub-chamber Volumetric Displacement [m³]	23.5×10^{-6}
Orifice count [-]	1
Orifice Area (Cross-section) [m²]	5.26×10^{-5}
Engine Cooling System [-]	Water Cooling with Heat Exchanger

Table 2 Specifications of the measurement instruments used in the experiments.

Measurement	Model	Measurement error
Pressure	Kistler 6054BR-3-1	±0.6%
Intake pressure	DELCO 3bar MAP Sensor	±1.5%
NO_x	Horiba MEXA-720NO_x	NO_x concentration within ±5% of output

Experimental Conditions and Procedure

We investigated the combustion characteristics and performance of ammonia/ethanol fuel blends in a high-compression-ratio spark-assisted compression ignition (SACI) engine equipped with a specialized sub-chamber design. The experimental setup shown in Table 3 was meticulously configured to ensure precise data collection, where the critical combustion parameters were recorded at intervals of 100 consecutive cycles to guarantee statistical reliability. Specifically, for the analysis of 100 recorded in-cylinder pressure cycles, only those with a peak pressure within three standard deviations of the mean were selected. We employed a dual-fuel injection system in which gaseous ammonia and liquid ethanol were introduced into the intake manifold via port fuel injection. This approach allowed precise control over the fuel blend composition while systematically varying two key parameters: (1) boost pressure at 5, 10, and 15 kPa (defined as the gauge pressure) and (2) ammonia energy ratio at 50 and 60%. In this experiment, the engine speed was controlled and the brake mean effective pressure (BMEP) under the conditions shown in Table 3 was varied within a range of 0.466–0.601 MPa. The ECU dynamically adjusted the ammonia energy ratio in real time and calibrated it according to the proportional contribution of the fuel to the total calorific value of the blend. To optimize combustion efficiency, the experimental design incorporated carefully timed valve events, with the specific intake and exhaust valve timings shown in Table 3.

Table 3 Investigated conditions for this study.

Fuels used in the experiment [-]	Ammonia, Ethanol
Ammonia Energy Ratio [%]	50, 60
Boost Pressure [kPa Gauge]	5, 10, 15
Ignition Timing [°CA BTDC (Compression Stroke)]	6
Standard Injection Timing [°CA ATDC (Intake Stroke)]	660
Brake Mean Effective Pressure (BMEP) [MPa]	0.466–0.601
Engine Speed [rpm]	1000
Excess Air Ratio [-]	1.2
Coolant Temperature [K]	343
Intake Air Temperature [K]	298
Intake Valve Opening (IVO) [°CA ATDC (Intake Stroke)]	-6
Intake Valve Closing (IVC) [°CA ATDC (Intake Stroke)]	215
Exhaust Valve Opening (EVO) [°CA ATDC (Intake Stroke)]	-218
Exhaust Valve Closing (EVC) [°CA ATDC (Intake Stroke)]	7

A constant ignition timing of 6 °CA BTDC was chosen for this experiment as it was able to achieve relatively stable combustion performance for higher ammonia energy ratios based on previous experiments focused on ignition timing variations (Okada et al., 2025). During the operation, a precisely metered portion of the air/ammonia/ethanol blend was routed into the sub-chamber during the compression phase. Ignition was initiated slightly before the top dead

DOI: 10.5614/j.eng.technol.sci.2026.58.6.1

center (TDC) of the compression stroke via a strategically positioned spark plug. The high-energy flame front generated in the sub-chamber then propagated into the main combustion chamber through a calibrated orifice during the power stroke, ensuring robust ignition of the primary charge.

Analytical Methods

Convection and radiation are the two main ways in which heat is transmitted during combustion from the cylinder interior to the walls. However, our analysis only considers convection heat transfer and we do not consider radiation heat transfer due to its insignificant effect on the spark ignition engine (Lounici & Bouzid., 2011). Thus, Eq. (1) can be used to determine $Q_{ht(\vartheta)}$, which is the heat transferred from combustion for every crank angle to the cylinder wall.

$$Q_{ht(\theta)} = h_{c(\theta)} A_c (T_{(\theta)} - T_w) \tag{1}$$

Here, $T_{(\vartheta)}$ corresponds to the in-cylinder temperature at every crank angle [K], and T_w corresponds to the average temperature of the wall cylinder [K]. A_c is the combustion chamber area [m²], and ϑ is the instantaneous crank angle position in degrees [°CA]. In addition, h_c is the convective heat transfer coefficient for gas [kW/m²K]. Hohenberg's correlation is expressed by Eq. (2) (Hohenberg, 1979), which serves as the foundation for the convective heat transfer coefficient, h_c.

$$h_{c(\theta)} = 1879 {P_{(\theta)}}^{0.8} {T_{(\theta)}}^{-0.4} {V_{(\theta)}}^{-0.06} \left(S_{(p)} + c\right)^{0.8} \tag{2}$$

Here, $V_{(\vartheta)}$ and $P_{(\vartheta)}$ represent the volume [m³] and in-cylinder pressure [MPa] at every crank angle, respectively. c represents the Hohenberg recommended calibration factor with a value of 1.4 (Hohenberg, 1979). Eq. (3) is used to calculate $\underline{S_p}$, which is the average speed of the piston [m/s].

$$S_P = 2S\frac{n}{60} \tag{3}$$

Here, n is the engine speed [rpm] and S is the piston stroke [m].

Eq. (4) is used to determine $Q_{HRR(\vartheta)}$, which is the heat release rate (HRR).

$$Q_{HRR(\theta)} = \frac{1}{\kappa - 1}\left(V_{(\theta)}\frac{dP}{d\theta} + \kappa P_{(\theta)}\frac{dV}{d\theta}\right) + Q_{ht} \tag{4}$$

Here, $\frac{dV}{d\theta}$ and $\frac{dP}{d\theta}$ are the rate of change of volume [m³] and pressure [MPa] in the main and sub-chamber for each crank angle, respectively, while κ is the specific heat ratio, which is defined as constant in this study. The collected data on the in-cylinder pressure can be used to calculate the IMEP. Eqs. (5) and (6) are used to calculate the IMEP.

$$IMEP = \frac{1}{V_s} \cdot \oint P dV \tag{5}$$

$$IMEP = \frac{1}{V_s} \cdot \sum_{\theta=0}^{a-1} \frac{P_{\theta+1} + P_\theta}{2} \cdot (V_{(\theta+1)} - V_{(\theta)}) \tag{6}$$

Here, a corresponds to the cumulative number of crank angles in a cycle, and V_s corresponds to the stroke volume [m³].

Eq. (7) is used to calculate the combustion duration.

$$Combustion\ Duration = CA90 - CA10 \tag{7}$$

Here, CA10 and CA90 are the crank angles at which 10 and 90% of the total heat has been released, respectively.

Eq. (8) is used to calculate the in-cylinder temperature [K].

$$T_{(\theta)} = \frac{P_{(\theta)} \cdot V_{(\theta)}}{P_{IVC} \cdot V_{IVC}} T_{IVC} \tag{8}$$

Here, T_{IVC}, P_{IVC}, and V_{IVC} are the temperature [K], pressure [MPa], and volume [m³] during intake valve closing (IVC), respectively.

Eq. (9) is used to calculate η_c, which is the combustion efficiency.

$$\eta_C = \frac{\int_{\theta_1}^{\theta_2} Q_{HRR} d\theta}{m_a \cdot H_{ua} + m_e \cdot H_{ue}} \tag{9}$$

Eq. (10) is used to determine η_i, which is the indicated thermal efficiency.

$$\eta_i = \frac{W_i}{m_a H_{ua} + m_e H_{ue}} \tag{10}$$

Here, m_e and m_a represent the fuel masses [kg] of the injected ethanol and ammonia, respectively. H_{ue} and H_{ua} represent the lower heating values [kJ/kg] of ethanol (26,700 kJ/kg) and ammonia (18,600 kJ/kg), respectively.

$$W_i = (W_C + W_P) \cdot 1000 \tag{11}$$

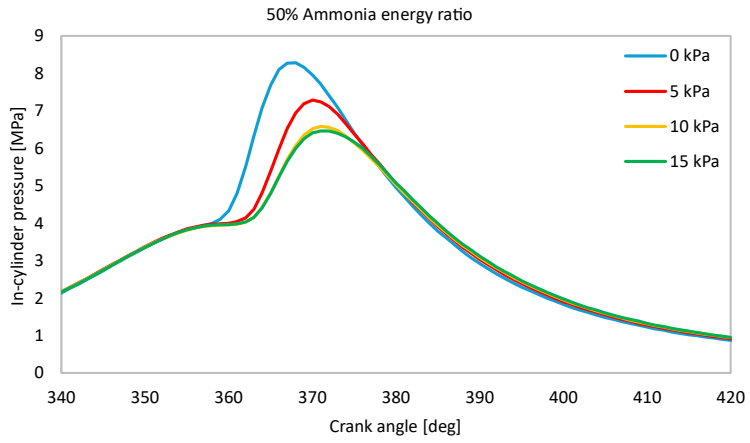
$$W_C = \int_{180^0}^{360^0} P\, dV \tag{12}$$

$$W_P = \int_{360^0}^{540^0} P\, dV \tag{13}$$

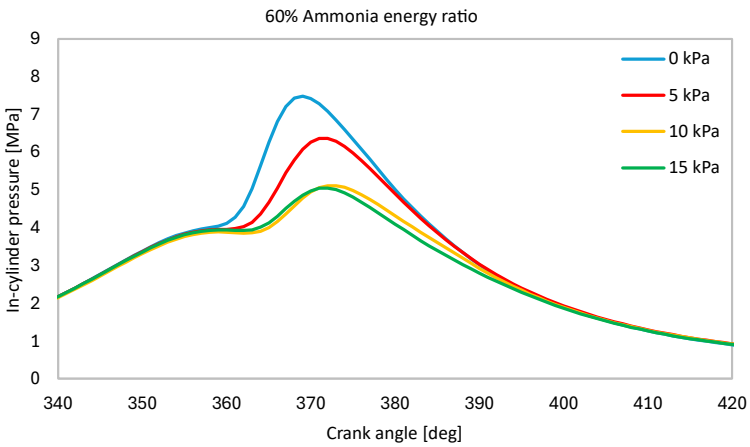
Here, W_i corresponds to the indicated work for each engine cycle [MJ]. W_C and W_P correspond to the amount of work required during the compression [MJ] and expansion [MJ] stages, respectively.

Experimental Results

In this section, the experimental results are presented and compared with previous results at 0 kPa (naturally aspirated condition) obtained using the same setup and operating conditions (Okada et al., 2025). Figure 2 compares the in-cylinder pressures at different boost pressures of 0, 5, 10, and 15 kPa for ammonia energy ratios of 50 and 60%. The results indicated that the in-cylinder pressure decreased with increasing intake pressure, where increasing the boost pressure from 0 to 5 kPa and from 5 to 10 kPa resulted in a substantial decrease in the in-cylinder pressure. However, a subsequent boost of 10 to 15 kPa had a minor effect on the measured in-cylinder pressure. The same behavior was observed for the heat release rate shown in Figure 3.



(a)



(b)

Figure 2 In-cylinder pressure against crank angle at various boost pressures for an ammonia energy ratio of (a) 50% and (b) 60%.

DOI: 10.5614/j.eng.technol.sci.2026.58.6.1

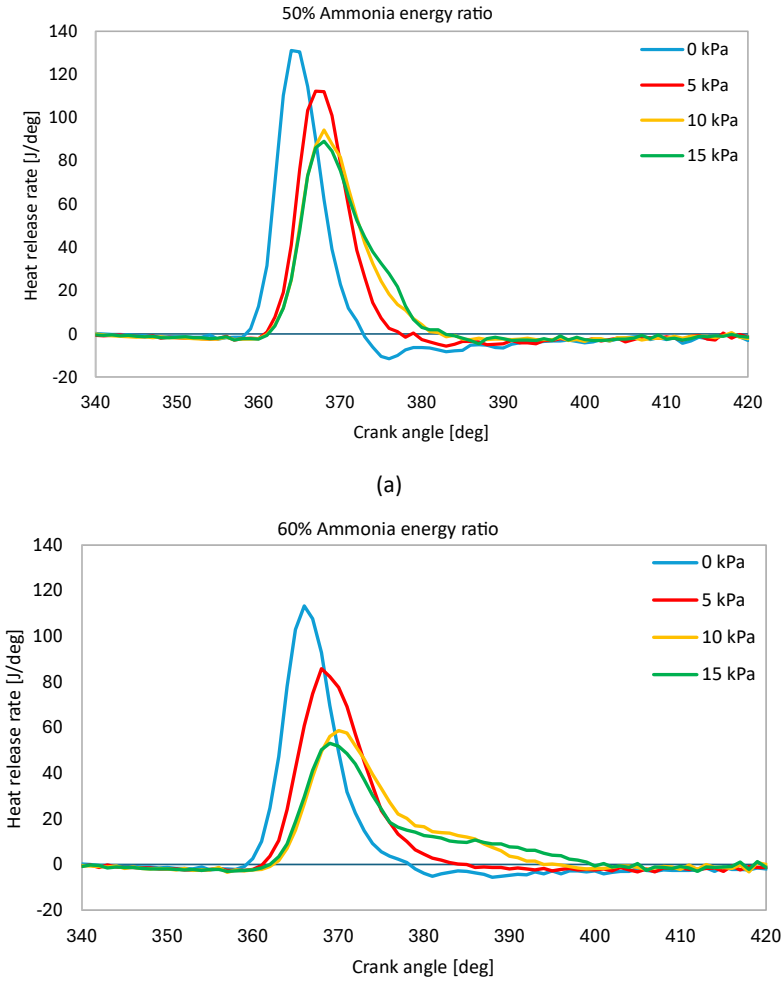


Figure 3 Heat release rate against crank angle at various boost pressures and ammonia energy ratios.

This decrease in the in-cylinder pressure and heat release rate with a higher intake boost can be attributed to the increased heat capacity of the fuel blend and high latent heat of vaporization of ethanol, which results in an enhanced charge cooling effect from ethanol evaporation (Pan et al., 2021; Khalif et al., 2017; Min et al., 2024) and reduces the overall combustion intensity. More details regarding this phenomenon are discussed in the following section. Furthermore, increasing the ammonia energy ratio to 60% resulted in both lower in-cylinder pressure and heat release rate due to slow flame speed and resistance to autoignition of ammonia, which prevented complete combustion.

Figure 4 shows the IMEP at various boost pressures of 0, 5, 10, and 15 kPa and ammonia energy ratios of 50 and 60%. The IMEP is a key metric for evaluating engine performance, representing the indicated work per unit stroke volume, as given by Eq. (6). The IMEP serves as a key indicator of how effectively an engine converts fuel energy into mechanical output. Although the results suggest a lower IMEP with a higher share of ammonia in the fuel blend (ammonia energy ratio: 60%), there seems to be a different dependence of IMEP on the intake boost for the two ammonia energy ratios investigated. At an ammonia energy ratio of 50%, varying the intake boost had a negligible effect on the engine IMEP. In contrast, a higher boost pressure reduced the IMEP for the engine operating with an ammonia energy ratio of 60%. The same behavior was also observed in the engine indicated thermal efficiency, as shown in Figure 5, because both are indicators of how effectively the engine uses energy, where the combination of an ammonia energy ratio of 50% and boost pressures of 0 kPa and 5 kPa yielded similar indicated thermal efficiency results.

The CoV, which is a metric used to evaluate combustion stability, is shown in Figure 6. While the values for an ammonia energy ratio of 50% suggest stable combustion (CoV < 5%), a significant increase in CoV was observed for an ammonia energy ratio of 60% at higher boost pressures (10 and 15kPa), which suggests instability during combustion. The possible reasons for such unstable operation include the slower reactivity of fuel blends with a higher ammonia energy ratio, which causes misfires during combustion. Although supercharging increases the intake air mass, it can also reduce the

effective intake charge temperature due to the enhanced charge cooling effects, particularly in fuels such as ethanol with a high latent heat of vaporization. The resulting lower in-cylinder temperature suppresses the reaction rates and further slows down the reactivity of the fuel blends, resulting in conditions that are more prone to combustion instability. To compensate for slower chemical kinetics and maintain optimal combustion phasing, earlier ignition timing is required. Therefore, we do not recommend using high boost pressures and high ammonia energy ratios for practical engines unless a more advanced ignition timing is used.

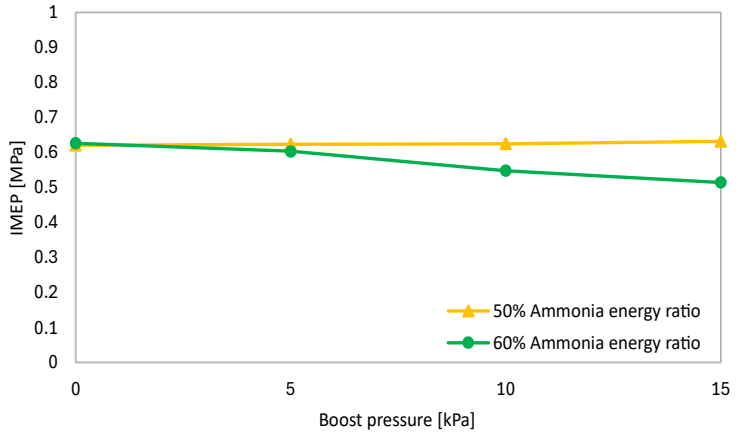


Figure 4 IMEP with respect to boost pressure at different ammonia energy ratios.

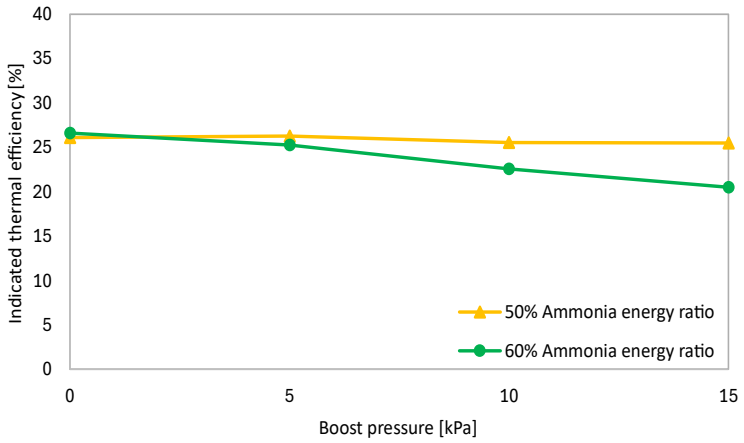


Figure 5 Indicated thermal efficiency for various boost pressures at different ammonia energy ratios.

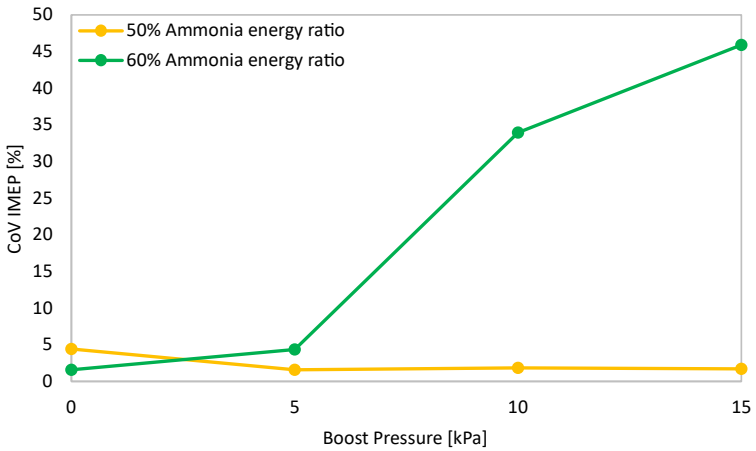


Figure 6 CoV IMEP for various boost pressures at different ammonia energy ratios.

DOI: 10.5614/j.eng.technol.sci.2026.58.6.1

Figure 7 compares the combustion duration for each experimental condition measured using the standard CA10–CA90 method, which calculates the crank angle between the points at which 10 and 90% of the total heat has been released, as defined in Eq. (7). The results show clear trends that help explain the behavior of ammonia/ethanol fuel blends during combustion under different engine settings. As expected, a higher ammonia content led to longer combustion times due to the high resistance of ammonia to combustion. The combustion duration is expected to follow the heat release rate behavior as the boost pressure is varied, as shown in Figure 3. Indeed, with an increased intake boost, the combustion duration was prolonged for both ammonia energy ratios, where the change was steep between boost pressures of 5 and 10 kPa for ammonia energy ratio of 50%. As for the cases with ammonia energy ratio of 60%, the same steep increase in duration was also observed when the boost pressure was increased from 10 kPa to 15 kPa.

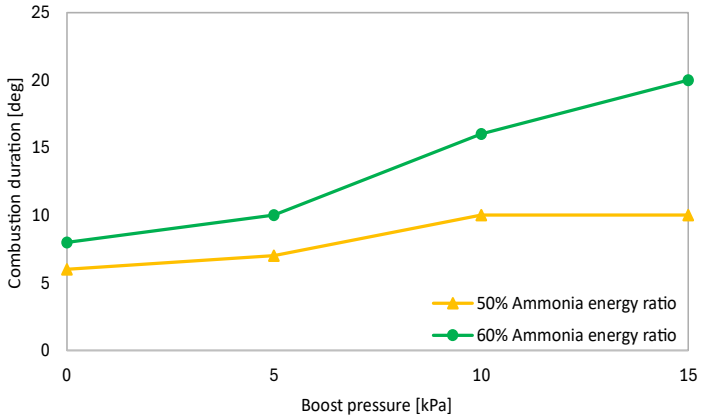


Figure 7 Combustion duration with respect to boost pressure at different ammonia energy ratios.

Figure 8 shows the combustion efficiency results calculated using Eq. (9). The combustion efficiency exhibited a trend consistent with the decrease in the in-cylinder pressure and heat release rate with increasing boost pressure. For an ammonia energy ratio of 50%, the combustion efficiency remained relatively stable, showing only a slight increase at 5 kPa, followed by a marginal decrease at higher boost pressures, indicating that the reduction in combustion intensity had a limited effect under this condition. Although boosting typically increases the intake air mass, the results indicate that this does not translate into improved combustion. Instead, increasing the boost pressure from 0 kPa to 10 kPa led to a reduction in the combustion efficiency, with only a minor additional effect observed from 10 kPa to 15 kPa, mirroring the decreasing changes observed in both the in-cylinder pressure and heat release rate. In contrast, for an ammonia energy ratio of 60%, the combustion efficiency decreased more noticeably with increasing boost pressure, reflecting the combined effects of reduced heat release and slower combustion kinetics associated with the higher ammonia content.

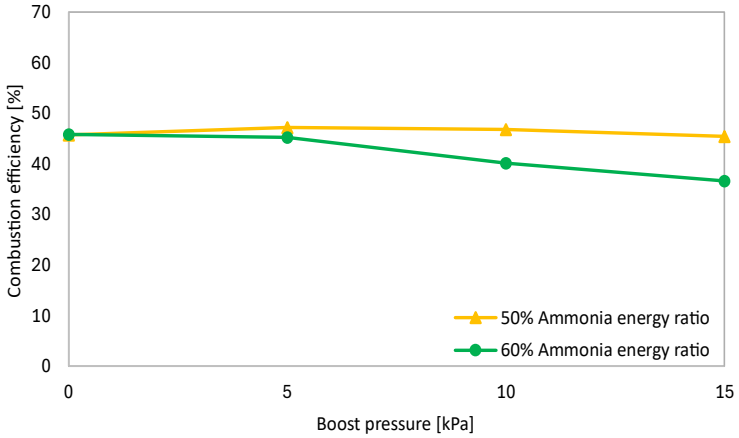


Figure 8 Combustion efficiency with respect to boost pressure at different ammonia energy ratios.

The in-cylinder temperatures for each condition determined using Eq. (8) are shown in Figure 9. In line with the heat release rate shown in Figure 3, the use of a higher boost pressure generated a lower in-cylinder temperature for the ammonia energy ratios investigated in this study. However, under all boost pressure conditions, the overall peak

temperature decreased as the ammonia energy ratio increased. Accordingly, the condition with the lowest boost pressure combined with the lowest ammonia energy ratio resulted in the highest combustion temperature. However, as shown in Figure 10, these conditions also generally corresponded to higher NO_x emissions. The reason for this tradeoff between performance and NO_x emissions is discussed in the following section.

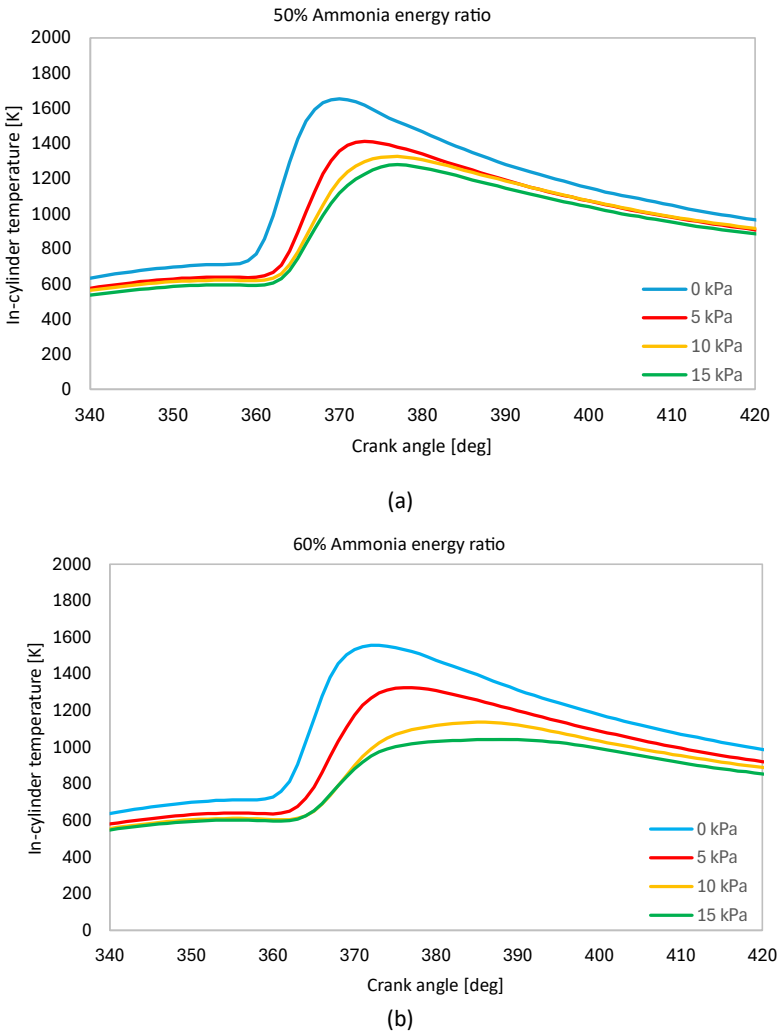


Figure 9 In-cylinder temperature against crank angle at various boost pressures and ammonia energy ratios.

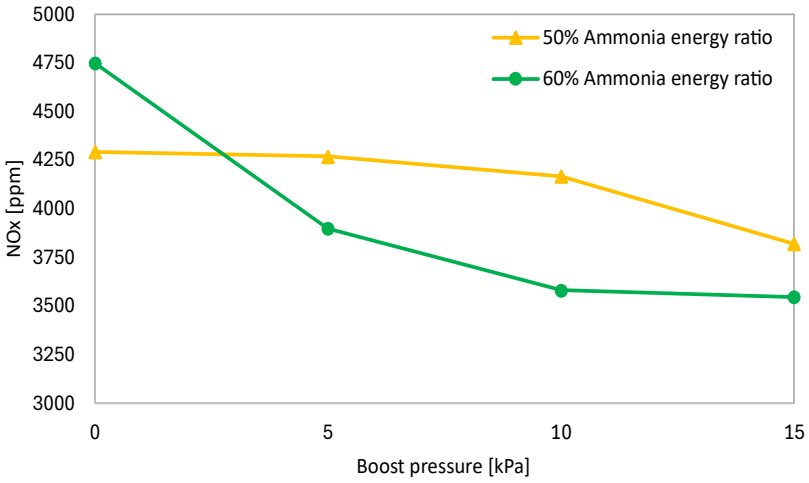


Figure 10 NO_x emissions with respect to boost pressure at different ammonia energy ratios.

DOI: 10.5614/j.eng.technol.sci.2026.58.6.1

Discussion

As shown in Figure 2, the peak in-cylinder pressure decreased and its occurrence was delayed to a later ignition timing with a higher boost pressure. When ethanol is subjected to high boost pressures, a significant amount of thermal energy is required to convert it from a liquid state to a vapor state. The absolute mass of injected ethanol increases to maintain the required energy ratio at higher boost pressures. The increased mass of the evaporating liquid extracts a substantial amount of sensible heat from the intake charge (Huang et al., 2015). This exact thermodynamic mechanism of increasing the mass of the injected ethanol enhances charge cooling. This energy requirement subsequently cools the combustion chamber, reducing the overall pressure development during combustion. This behavior is interesting because it differs significantly from that of conventional hydrocarbon fuels, such as gasoline and diesel, where a higher boost pressure usually results in a higher cylinder pressure due to enhanced volumetric efficiency (Anggono et al., 2019). The overall cylinder pressure appeared to be affected by variations in the ammonia energy ratio. A lower ammonia energy ratio generated higher peak pressures than a higher ammonia energy ratio for all boost pressures investigated in this study. The presence of more ethanol promotes the formation of radicals, which accelerate the reaction process, leading to shorter ignition delay times and a higher overall flame speed (Li et al., 2023; Yang et al., 2024; Pelé et al., 2022). This agrees with the results shown in Figure 7, where the combustion duration is prolonged at a higher ammonia energy ratio.

As shown in Figure 3, increasing the boost pressure consistently resulted in lower peak heat release rates for all ammonia energy ratios. It is evident that there is an inverse relationship between the boost pressure and maximum heat release rate when using ammonia-dominant fuel blends, and that this trend is consistent with the in-cylinder pressure behavior shown in Figure 2, indicating a consistent thermodynamic response across the various measurement parameters. Analysis of the results also revealed a clear and consistent pattern in the combustion properties between different ammonia energy ratios. Varying the ammonia energy ratio resulted in a behavior similar to the boost pressure effect, where a lower ammonia energy ratio combined with a lower boost pressure corresponded to higher peak heat release rates. The higher heat release with a lower ammonia energy ratio can be attributed to the increased combustibility of the fuel blend due to the greater proportion of ethanol in the fuel blend, which is more combustible than ammonia. This effect was more pronounced at lower boost pressures, where the cooling effects of ethanol vaporization were lower. Such a noticeable decrease in peak heat release rate observed after switching from an ammonia energy ratio of 50% to 60% emphasizes the need for fuel ratio adjustments in order to attain optimal combustion performance.

As shown in Figure 4, the fuel blend with an ammonia energy ratio of 60% produced lower IMEP values across all tested boost pressures compared with those with an ammonia energy ratio of 50%. This reduction in performance is due to the inherent combustion properties of ammonia. Ammonia has a naturally slow laminar flame speed, which causes it to burn slower than ethanol (Dong et al., 2024). Therefore, the combustion process is slower and less complete when more ammonia is used, particularly during the power stroke, where pressure generation is the most critical. A slower burn rate results in lower in-cylinder pressures, which ultimately lead to a reduction in the overall work that an engine can produce per cycle. Furthermore, the influence of boost pressure on the IMEP varied depending on the ammonia content of the fuel. For an ammonia energy ratio of 60%, increasing the boost pressure from 0 kPa to 15 kPa resulted in a gradual decrease in the IMEP. In contrast, an ammonia energy ratio of 50% showed a more stable response, maintaining relatively consistent IMEP values regardless of the boost pressure applied. The decrease in the IMEP with increasing boost pressure is caused by the high latent heat of vaporization of ethanol (Pan et al., 2021; Khalif et al., 2017; Min et al., 2024), which absorbs a large amount of heat as it evaporates. At higher boost pressures, this effect becomes stronger, which leads to cooling of the intake charge and combustion chamber. This cooling effect reduces the amount of thermal energy available to create pressure during combustion. The different responses to the boost pressure between ammonia energy ratios of 50 and 60% can be attributed to the reactivity of the fuel blend. Because ammonia has a significantly slower flame speed than ethanol, a higher ammonia content slows down combustion, and combined with the boost pressure (where cooling due to ethanol evaporation is more intense) worsens the combustion performance. The most significant drop in IMEP occurred when the boost pressure was increased from 5 kPa to 10 kPa and the IMEP further decreased at higher boost pressures combined with an ammonia energy ratio of 60%. In this case, the IMEP was lower than that without boost pressure. Furthermore, as shown in Figure 6, the reduced performance under this condition was followed by a significant increase in the CoV IMEP above 5%, indicating unstable engine operation. This highlights the challenges of using ethanol paired with high-ammonia-content fuels under high boost pressures.

As shown in Figure 5, the indicated thermal efficiency decreased, which was consistent with the increasing ammonia energy ratios. Although significant decrease in the indicated thermal efficiency was not observed at an ammonia energy

ratio of 50% with increasing boost pressure, a noticeable decrease in the indicated thermal efficiency was evident at an ammonia energy ratio of 60%. This difference in performance can be attributed to several factors. The slow-burning characteristic of ammonia makes combustion less efficient, and the high latent heat of vaporization of ethanol absorbs a large amount of heat during evaporation. At a higher boost pressure, this cooling effect becomes stronger, thereby reducing the combustion temperature and energy output. This cooling effect leads to greater heat loss from the combustion chamber, further reducing the thermal efficiency. When a higher ammonia energy ratio is combined with a higher boost pressure, the combustion performance worsens. The slow burning of ammonia and the strong cooling effects of ethanol vaporization work together concurrently, which reduces the combustion effectiveness and efficiency. The engine setup used in this study benefits from the incorporation of a higher ethanol content, which helps the fuel to burn faster and more completely, whereas the low boost pressure reduces the cooling effect from ethanol evaporation. In combination, these factors help the engine convert more of the fuel blend's energy into useful work, leading to higher efficiency.

Figure 7 shows the trend of the combustion duration of the fuel mixture, which further supports the combustion behavior of ammonia, showing that the combustion duration is primarily governed by the low combustion speed of ammonia, as noted in an earlier study (Dong et al., 2024). As shown in Figure 3(a), when comparing the results at boost pressures of 5 and 10 kPa, the peak heat release rate at 10 kPa was smaller than that at 5 kPa. The heat release rate of ~375–380 °CA at 10 kPa was more pronounced than that at 5 kPa. This resulted in slower combustion and an increase in combustion duration. However, when comparing the results at boost pressures of 10 and 15 kPa, the characteristics of the heat release rate for both cases were similar, resulting in a similar combustion duration. As shown in Figure 7, when the ammonia energy ratio was 60%, the combustion duration increased in the order of increasing boost pressure (5 → 10 → 15 kPa). As shown in Figure 3(b), this is due to the decrease in the peak heat release rate in the above order. This is also evident when comparing the overall heat release at boost pressures of 5 and 10 kPa, where a delay ~385 °CA to 395 °CA was observed for the end of heat release. Subsequently, when comparing the results at boost pressures of 10 and 15 kPa, a further delay of ~395 °CA to 400 °CA was observed. These factors result in slower combustion and longer combustion duration. The slower burning rate of ammonia causes heat to be released more gradually, which stretches out the entire combustion process. The results showed that increasing the boost pressure from 0 kPa to 15 kPa also led to longer combustion times for both fuel blends. This is due to ethanol's high latent heat of vaporization (Pan et al., 2021; Khalif et al., 2017; Min et al., 2024). This characteristic enables ethanol to absorb heat during evaporation. At higher boost levels, this effect becomes stronger, cooling the air/fuel mixture and delaying the start and progress of combustion. This cooling effect helps explain the observed decrease in the peak heat release rate and peak cylinder pressure as the boost pressure increases. The combination of a higher ammonia energy ratio and applying a high boost pressure had an even more noticeable effect. Although both ammonia energy ratios of 50 and 60% showed longer combustion durations at higher boost levels, the fuel blend with an ammonia energy ratio of 60% was more sensitive to these changes. At the highest boost pressure of 15 kPa, the fuel blend with an ammonia energy ratio of 60% had a significantly longer combustion duration than that with an ammonia energy ratio of 50% under the same conditions. This increased sensitivity for the fuel blend with a higher ammonia energy ratio is also caused by the same two factors affecting the combustion of ammonia: the high ignition temperature and slow flame speed. Indeed, the slow burning speed of ammonia and strong cooling of ethanol during vaporization under pressure are the factors that significantly contribute to slower combustion for the fuel blend with a higher ammonia energy ratio.

To further clarify the combustion duration under supercharging conditions, the combustion phase was analyzed using CA0–10, CA50, and CA10–90, which represent the ignition delay, combustion center, and combustion duration, respectively. The observed combustion phases are shown in Figure 11. As the boost pressure increased, the CA0–10 values showed a were relatively constant when using an ammonia energy ratio of 50%, suggesting a more stable initial combustion. In contrast, a slight increase in CA0-10 values was observed for cases with an ammonia energy ratio of 60% and higher boost pressure, suggesting a minor extension of the ignition delay. This behavior is thought to be due to the suppression of initial heat generation through a combination of effects such as enhanced intake air cooling and decreased chemical reactivity of the ammonia/ethanol fuel blend. The results for CA50 showed relatively constant crank angle values when the boost pressure was increased and an ammonia energy ratio of 50% was used. In contrast, the CA50 values slightly increased for an ammonia energy ratio of 60% at higher boost pressures, which could reduce the overall combustion efficiency. Because CA50 represents the heat generation center, this delay implies that a large part of the combustion occurs later than the optimal timing. Therefore, the decrease in IMEP observed under supercharging conditions is identified as being mainly caused by the delay in the combustion phase. These results are also reflected in the respective combustion efficiency and indicated thermal efficiency results. In addition, the CA10–90 values increased when a higher boost pressure was applied. This effect was more notable at an ammonia energy ratio of 60%, in contrast to that at an ammonia energy ratio of 50%. This trend indicates prolonged combustion duration and reduced work done during the expansion stroke, which accounts for the decrease in the IMEP and directly affects the decrease in thermal

DOI: 10.5614/j.eng.technol.sci.2026.58.6.1

efficiency. One possible explanation for this is that the cooling effect associated with ethanol further slows down the oxidation reactions, which are already slow during the combustion of ammonia. Therefore, the cooling effect caused by ethanol evaporation and its influence are considered as follows: When the boost pressure is increased from 5 kPa to 15 kPa, the difference in ethanol injection mass is 1.29×10^{-6} and 1.57×10^{-6} kg for an ammonia energy ratio of 50 and 60%, respectively. Assuming a latent heat of vaporization of ethanol of 838 kJ/kg and a specific heat of air of 1.006 kJ/kgK as the main content of the blend, and further assuming that the entire displacement volume of 6.38×10^{-4} m^3 is cooled, the increase in boost pressure from 5 kPa to 15 kPa results in an additional temperature drop of 1.3 and 1.6 K for an ammonia energy ratio of 50 and 60%, respectively. This decrease in temperature at the intake timing becomes substantial at a later stage when the fuel blends undergo compression. Furthermore, the above analysis assumes a fully homogenous blend and cooling of the entire intake charge, whereas in actual conditions, the fuel blend may not be fully homogenous at the intake timing, which can result in a larger reduction in the local temperature.

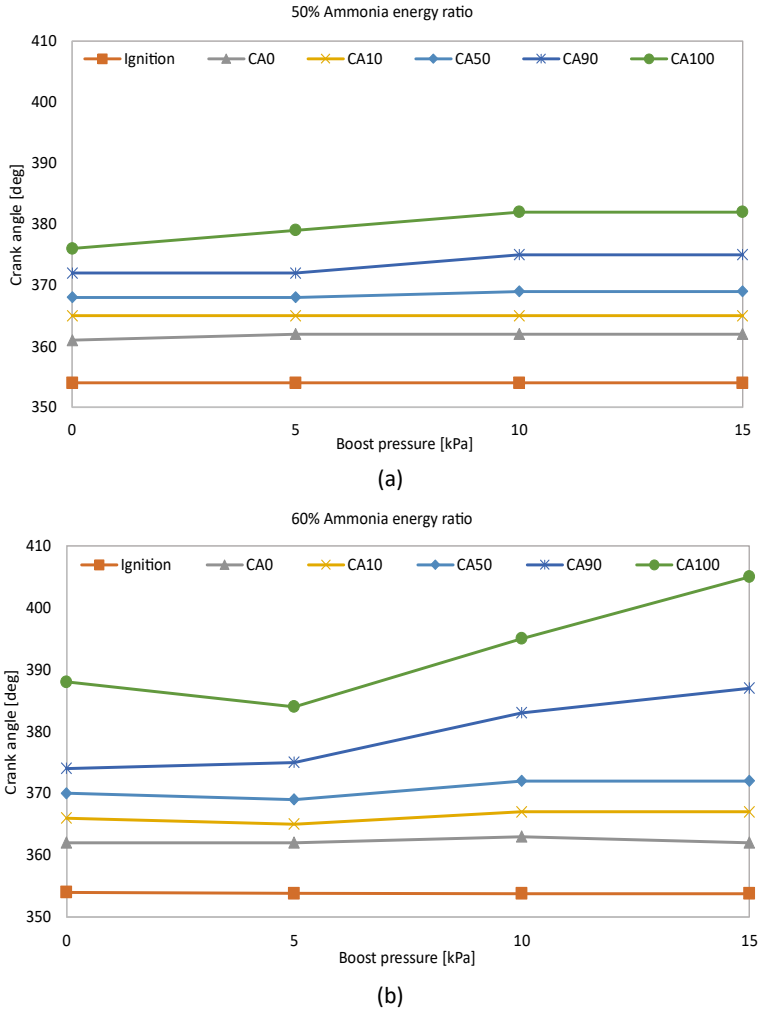


Figure 11 Combustion phasing with respect to boost pressure at different ammonia energy ratios.

The combustion efficiency results can be observed in Figure 8, where the resulting trend can be attributed to the enhanced charge cooling effect caused by the high latent heat of vaporization of ethanol, which reduces the in-cylinder temperature and suppresses the reaction rates, thereby reducing both the in-cylinder pressure and heat release. As the boost pressure increases, more air/fuel mixture is introduced into the cylinder, resulting in a larger amount of heat energy required to evaporate ethanol. This absorbs a significant amount of heat from the surrounding charge, leading to a reduction in the in-cylinder temperature before ignition. An increase in the ammonia energy ratio further reduces the thermal efficiency due to the low reactivity of ammonia and slow flame propagation, which prevents complete combustion. When these two effects are combined, the combustion duration is significantly extended, which explains the substantial decrease in the combustion efficiency. In contrast, at an ammonia energy ratio of 50%, a higher fraction of ethanol enhances the reactivity, allowing combustion efficiency to remain steady despite the cooling effect. Overall, the above observations suggest that increasing the boost pressure under the investigated conditions does not lead to

an increase in the combustion performance, but instead contributes to reduced efficiency, particularly at higher ammonia fractions.

Figures 9 and 10 show the relationships between the boost pressure, ammonia energy ratio, in-cylinder temperature, and NO_x emissions. The trend observed in Figure 9 may be associated with the high latent heat of vaporization of ethanol (Pan et al., 2021; Khalif et al., 2017; Min et al., 2024). A slight decrease in the overall cylinder temperature was observed as the boost pressure was increased for all ammonia energy ratios used in this study. The combination of increased mixture heat capacity, strong charge cooling effect from ethanol evaporation, and slow combustion kinetics of ammonia results in a reduction in the peak heat release rate, which leads to a lower estimated combustion temperature. With this observation, it is reasonable to infer that the thermal NO_x formation from atmospheric nitrogen is also suppressed by the lower combustion temperature (Qian et al., 2024). Indeed, a decreasing trend in NO_x emissions was observed as the boost pressure increased for all ammonia energy ratios, which was consistent with the lower in-cylinder temperature observed at higher boost pressures, as shown in Figure 9. The opposite behavior was observed for the effect of ammonia energy content, where a higher ammonia energy ratio generally resulted in lower NO_x emissions under boosted conditions. However, unlike hydrocarbons, where NO_x is mainly formed from atmospheric nitrogen, which is dependent on the combustion temperature, the presence of nitrogen in the molecular structure of ammonia can promote the formation of NO_x during combustion, and hence, a higher ammonia energy ratio is expected to promote NO_x emissions. Nonetheless, as shown in Figure 10, with the exception of the naturally aspirated case, higher ammonia energy ratios resulted in lower NO_x emissions. This trend is consistent with less effective combustion at higher ammonia energy ratios, which may reduce NO_x formation and leave more residual NH_3 available to react with NO_x to form nitrogen and water vapor (Tian et al., 2024), which is commonly referred to as the thermal $DeNO_x$ process. However, because ammonia slip was not directly measured in this study, the presence and contribution of such reactions cannot be confirmed. Therefore, the observed reduction in NO_x emissions is discussed primarily in relation to the combined effects of the combustion temperature and fuel properties. However, this interpretation does not directly apply to the naturally aspirated case (boost pressure: 0 kPa) because combustion is more effective and the in-cylinder temperature is substantially higher than that in the boosted cases, potentially resulting in less residual NH_3 available for NO_x reduction while also promoting thermal NO_x formation (Okada et al., 2025). Accordingly, a higher ammonia energy ratio resulted in higher NO_x emissions under naturally aspirated condition (boost pressure: 0 kPa).

$$4\mathrm{NO} + 4\mathrm{NH_3} + \mathrm{O_2} \rightarrow 4\mathrm{N_2} + 6\mathrm{H_2O} \quad (14)$$

$$NO + NO_2 + 2NH_3 \rightarrow 2N_2 + 3H_2O \quad (15)$$

$$6NO_2 + 8NH_3 \rightarrow 7N_2 + 12H_2O \quad (16)$$

Conclusion

Based on the key findings of this study, several conclusions can be drawn regarding the combustion performance of ammonia/ethanol blends. First, a higher ammonia energy ratio resulted in slower ignition due to the high ignition temperature and slow flame speed of ammonia, which was reflected in the peak heat release rate, in-cylinder pressure, and engine efficiency that directly correlates with the indicated thermal efficiency; consequently, a better overall performance was achieved using a lower ammonia energy ratio of 50%. Furthermore, increasing the boost pressure decreased the peak heat release rate and in-cylinder pressure because the high latent heat of vaporization of ethanol increased the thermal energy required for fuel vaporization, subsequently cooling the engine and decelerating combustion. Across all ammonia energy ratios, applying a higher boost pressure reduced the overall engine performance, as evidenced by the IMEP and indicated thermal efficiency, while combining a high boost pressure with a high ammonia energy ratio led to unstable combustion and misfires due to slower blend reactivity, highlighting the need for more advanced ignition timing and indicating that optimal results are achieved at the lowest boost pressure.

In addition to altering overall performance, a higher ammonia energy ratio demanded higher temperatures to initiate combustion and exhibited slower flame propagation that prolonged the combustion duration. This duration was extended even further by increasing the boost pressure—particularly at higher ammonia energy ratios due to the combined effects of the high boost pressure and ethanol's high latent heat of vaporization cooling the chamber, it suggests that combining a lower ammonia energy ratio with the lowest boost pressure yields the shortest combustion duration. Regarding exhaust characteristics, variations in boost pressures and ammonia energy ratios significantly altered NO_x emission levels. Higher boost pressures lowered overall NO_x emissions across all blends due to reduced in-cylinder temperatures, whereas higher ammonia energy ratios also reduced NO_x emissions, likely driven by the thermal $DeNO_x$ process where excess unburned NH_3 reacts with NO_x. Thus, a distinct trade-off exists between engine performance and emissions, wherein the combination of the lowest boost pressure and the lowest ammonia energy

DOI: 10.5614/j.eng.technol.sci.2026.58.6.1

ratio delivered superior performance but generated the highest NO_x emissions among the tested conditions. Overall, this study demonstrates the necessity of carefully optimizing both boost pressure and ammonia energy ratio for practical application, and future research is recommended to investigate other operating parameters such as ignition timing, engine speed, intake temperature, and excess air ratio under boosted conditions to achieve both enhanced engine performance and reduced NO_x emissions.

Acknowledgments

This research was supported by the Japan Society for the Promotion of Science, Grants-in-Aid for Scientific Research (No.19K04244), Sophia University, and Petra Christian University (project code 097/PSTM/ST/2023) as part of an international collaborative project. The authors gratefully acknowledge the support of these institutions.

Compliance with ethics guidelines

The authors declare they have no conflict of interest or financial conflicts to disclose.

This article contains no studies with human or animal subjects performed by the authors.

References

Anggono, W., Ikoma, W., Chen, H., Liu, Z., Ichiyanagi, M., & Suzuki, T. (2019). Effect of various supercharger boost pressure to in-cylinder pressure and heat release rate characteristics of direct injection diesel engine at various engine rotation. *E3S Web of Conferences, 130*, 01036. https://doi.org/10.1051/e3sconf/201913001036

Brandon, N., & Smith, J. (2021). The role of hydrogen and ammonia in meeting the net zero challenge (Briefing 4, pp. 1–13). The Royal Society. Retrieved February 15, 2025, from https://royalsociety.org/-/media/policy/projects/climate-change-science-solutions/climate-science-solutions-hydrogen-ammonia.pdf

Ding, Y., Pan, G., Han, D., & Huang, Z. (2025). Combustion and emissions of an ammonia-gasoline dual-fuel spark ignition engine: Effects of ammonia substitution rate and spark ignition timing. *International Journal of Hydrogen Energy*, *122*, 348–358

Dong, P., Zhang, C. Y., & Wang, J. Y. (2024). Future zero carbon ammonia engine: Fundamental study on the effect of jet ignition system characterized by gasoline ignition chamber. *Journal of Cleaner Production, 435*, 140546. https://doi.org/10.1016/j.jclepro.2023.140546

Guo, B., Ichiyanagi, M., Kajiki, K., Aratake, N., Zheng, Q., Kodaka, M., & Suzuki, T. (2022). Combustion analysis of ammonia-fueled high compression ratio SI engine with glow plug and sub-chamber: Effects of ammonia content under condition of co-combustion with gasoline/ammonia/air. *International Journal of Automotive Engineering, 13*(1), 1–8. https://doi.org/10.20485/JSAEIJAE.13.1_1

Hamedani, A. E., & Abbasian, A. (2024). Hydrogen as an energy source: A review of production technologies and challenges of fuel cell vehicles. *Energy Reports, 12*, 3778–3794. https://doi.org/10.1016/j.egyr.2024.09.030

Hayakawa, A., Kobayashi, H., & Kudo, T. (2015). Laminar burning velocity and Markstein length of ammonia/air premixed flames at various pressures. *Fuel, 159*, 1–7. https://doi.org/10.1016/j.fuel.2015.06.070

Hohenberg, G. F. (1979). Advanced approaches for heat transfer calculations. SAE Technical Papers. https://doi.org/10.4271/790825

Hu, L., Wang, Y., & Zhang, J. (2024). Quantitative analysis of toxicity risks in the operation of ammonia-fueled tugboats. *Ocean Engineering, 310*, 118759. https://doi.org/10.1016/j.oceaneng.2024.118759

Huang, Y., Hong, G., & Huang, R. (2015). Investigation to charge cooling effect and combustion characteristics of ethanol direct injection in a gasoline port injection engine. *Applied Energy*, *160,* 244-254. https://doi.org/10.1016/j.apenergy.2015.09.059

Ichiyanagi, M., Yilmaz, E., Suzuki, T., Okada, T., Yamamoto, H., Kodaka, M., Shiraishi, H., Mukae, S., Tamba, R., Widjaja, H., Jonathan, L., Gunawan, S., Gotama, G. J., & Anggono, W. (2024a). Combustion analysis of ammonia/gasoline mixtures at various injection timing conditions in a high compression ratio SI engine with sub-chamber. *Automotive Experiences, 7*(2), 321–332. https://doi.org/10.31603/ae.10533

Ichiyanagi, M., Yilmaz, E., Ohashi, T., Sanno, M., Lin, G., Gunawan, S., Widjaja, H., Jonathan, L., Gotama, G. J., Anggono, W., & Suzuki, T. (2024b). Experimental Investigation of Ammonia/Oxygen/Argon Combustion: The Role of Equivalence Ratio and Nozzle Shape in a Constant Volume Combustion Chamber with Sub-chamber. *Journal of Engineering and Technological Sciences*, *56*(6), 704–715. https://doi.org/10.5614/j.eng.technol.sci.2024.56.6.3

Khalif, E., Tabataba, M., Demirkhan, A., & Aghbashlo, A. (2017). Impacts of additives on performance and emission characteristics of diesel engines during steady-state operation. *Progress in Energy and Combustion Science, 59*(201), 32–58.

Kumar, M., Singh, R., & Gupta, A. (2024). Statistical investigation of combustion and emission characteristics of biofuels according to their physical properties: A way to explore suitable alternative fuels. *Fuel, 358,* 130242. https://doi.org/10.1016/j.fuel.2023.130242

Lanni, D., & Rossi, M. (2022). Assessment of the operation of an SI engine fueled with ammonia. *Energies, 15*(22), 8583. https://doi.org/10.3390/en15228583

Lanni, D., D'Antuono, G., Galloni, E., Fontana, G., Contino, F., & Brequigny, P. (2025). Improving ammonia combustion in spark-ignition engines coupling hydrogen enrichment with multiple spark plugs. *Energy & Fuels, 39*(14), 7137–7150. https://doi.org/10.1021/acs.energyfuels.5c00320

Li, M., Zhu, D., He, X., Moshammer, K., Fernandes, R. X., & Shu, B. (2023). Experimental and kinetic modeling study on auto-ignition properties of ammonia/ethanol blends at intermediate temperatures and high pressures. *Proceedings of the Combustion Institute, 39*(1), 511-520. https://doi.org/10.1016/j.proci.2022.07.151

Lounici, M. S., & Bouzid, A. (2011). Investigation on heat transfer evaluation for a more efficient two-zone combustion model in the case of natural gas SI engines. *Applied Thermal Engineering, 31*(2–3), 1234–1242. https://doi.org/10.1016/j.applthermaleng.2010.09.012

Meng, X., Zhang, Y., & Li, J. (2024). Effects of ammonia addition and variable valve timing on knocking and engine performance of an ethanol pre-chamber engine with high compression ratio. *Energy, 327*, Article 136342. https://doi.org/10.1016/j.energy.2025.136342

Min, S.-H., & Suh, H.-K. (2024). The Effect of Combustion Phase According to the Premixed Ethanol Ratio Based on the Same Total Lower Heating Value on the Formation and Oxidation of Exhaust Emissions in a Reactivity-Controlled Compression Ignition Engine. *Fire, 7*(7), 258. https://doi.org/10.3390/fire7070258

Mohammed, A. G., Zhang, Y., & Li, J. (2024). Review on the ammonia-blend as an alternative fuel for micro gas turbine power generation. *International Journal of Hydrogen Energy, 82,* 428–447. https://doi.org/10.1016/j.ijhydene.2024.07.396

Moriarty, P., & Honnery, D. (2019). Prospects for hydrogen as a transport fuel. *International Journal of Hydrogen Energy, 44*(31), 16029–16037. https://doi.org/10.1016/j.ijhydene.2019.04.278

Okada, T., Ichiyanagi, M., Yilmaz, E., Suzuki, T., Shiraishi, H., Ngwompe Souop, E. L. R., Widjaja, E., Sutedjo, J., Marcelo, C. D., Tjiotijono, F. R., Gotama, G. J., & Anggono, W. (2025). The effect of ignition timing on combustion of ammonia/ethanol mixtures in spark-assisted compression ignition engine with a sub-chamber. *Journal of Engineering and Technological Sciences, 57*(6), 735–746. https://doi.org/10.5614/j.eng.technol.sci.2025.57.6.1

Pan, J., Chen, B., Tao, J., Fan, B., Liu, J., Li, Y., & Otchere, P. (2021). Experimental investigation on the effect of ethanol blending on gasoline combustion characteristics and idle performance in a rotary engine. *International Journal of Thermal Sciences, 30*, 1187–1198. https://doi:10.1007/s11630-021-1487-3

Pelé, R., Brequigny, P., Bellettre, J., & Mounaïm-Rousselle, C. (2024). Performances and pollutant emissions of spark ignition engine using direct injection for blends of ethanol/ammonia and pure ammonia. *International Journal of Engine Research*, *25*(2), 320–333.

Pelé, R., Brequigny, P., Mounaim-Rousselle, C., Dayma, G., & Halter, F. (2022). Laminar flame speed of ethanol/ammonia blends—An experimental and kinetic study. *Fuel Communications, 10,* Article 100052. https://doi.org/10.1016/j.jfueco.2022.100052

Qian, F., Zhang, S., Wang, J., Zhu, N., Bao, X., Yang, H., Xu, X., Alshahrani, W. A., Helal, M. H., & Guo, Z. (2024). Ammonia energy fraction effect on the combustion and reduced NO_x emission of ammonia/diesel dual fuel. *Environmental Research, 261*, Article 119530. https://doi.org/10.1016/j.envres.2024.119530

Sapnken, F. E., Tamba, J. G., Essiane, N., Koffi, F. D., & Njomo, D. (2024). The potential of green hydrogen fuel as an alternative in Cameroon's road transport sector. *International Journal of Hydrogen Energy, 49*, 433–449. https://doi.org/10.1016/j.ijhydene.2023.08.339

Shih, C. F., Zhang, T., Li, J., & Bai, C. (2018). Powering the future with liquid sunshine. *Joule*, *2*(10), 1925–1949. https://doi.org/10.1016/j.joule.2018.08.016

Sonawane, S., Sekhar, R., Warke, A., Thipse, S., Rairikar, S., & Varma, C. (2025). Experimental Investigation and Prediction of Combustion Parameters using Machine Learning in Ethanol - Gasoline Blended Engines. *Journal of Engineering and Technological Sciences*, *57*(1), 27–47. https://doi.org/10.5614/j.eng.technol.sci.2025.57.1.3

Sun, J., Tang, Q., Wen, M., Huang, L., Liu, H., & Yao, M. (2024). Combustion characteristics and flame development of ammonia in an optical spark ignition engine. *Fuel, 359*, Article 129904.

Tian, J., Wang, L., Xiong, Y., Wang, Y., Yin, W., & et al. (2024). Enhancing combustion efficiency and reducing nitrogen oxide emissions from ammonia combustion: A comprehensive review. *Process Safety and Environmental Protection, 183,* 514–543. https://doi.org/10.1016/j.psep.2024.01.020

Uddeen, K., Tang, Q., Shi, H., & Turner, J. (2024). Performance and emission analysis of ammonia-ethanol and ammonia-methane dual-fuel combustion in a spark-ignition engine: An optical study. *Fuel, 358*, 130296. https://doi.org/10.1016/j.fuel.2023.130296

DOI: 10.5614/j.eng.technol.sci.2026.58.6.1

Uddeen, K., Tang, Q., Shi, H., Magnotti, G., & Turner, J. (2023). A novel multiple spark ignition strategy to achieve pure ammonia combustion in an optical spark-ignition engine. *Fuel*, *349*, 128741. https://doi.org/10.1016/j.fuel.2023.128741

United States Environmental Protection Agency. (2023). Global greenhouse gas emissions data. Retrieved February 15, 2025, from https://www.epa.gov/ghgemissions/global-greenhouse-gas-emissions-data

Yang, H., Tian, J., Cui, Z., Ye, M., Zhang, X., Zhou, Q., Wei, K., & Wang, J. (2024). Experimental and numerical study of combustion characteristics of ammonia/ethanol mixture under high temperature and pressure. *Fuel, 367,* Article 131350. https://doi.org/10.1016/j.fuel.2024.131350

Yilmaz, E., Ichiyanagi, M., Zheng, Q., Guo, B., Aratake, N., Kodaka, M., Shiraishi, H., Okada, T., & Suzuki, T. (2023). Investigation of intake air temperature effect on co-combustion characteristics of NH_3/gasoline in naturally aspirated high compression-ratio engine with sub-chamber. *Scientific Reports, 13*(1), 11649. https://doi.org/10.1038/s41598-023-38883-3

Zhang, B., Rubio, M., Egolfopoulos, F., & Cronin, S. B. (2025). Stable combustion of ammonia in an internal combustion engine: A single fuel approach enabled by multi-pulse transient plasma ignition. *Fuel*, *381*, 133502. https://doi.org/10.1016/j.fuel.2024.133502

Zhu, G., Liu, X., & Chen, Y. (2024). Optical diagnostic study of ammonia-kerosene dual-fuel engine combustion process. *International Journal of Hydrogen Energy, 81,* 110–126. https://doi.org/10.1016/j.ijhydene.2024.07.256

Manuscript Received: 26 November 2025
Revised Manuscript Received: 4 April 2026
Accepted Manuscript: 22 July 2026